

Design of Rotor Magnetic Barrier Structure of Built-in Permanent Magnet Motor Based on Taguchi Method

Shengnan Wu, *Member, IEEE*, Xianwen Pang, Wenming Tong, *Member, IEEE*, and Yingcong Yao

Abstract—In this paper, a 20kW vehicle built-in permanent magnet synchronous motor is taken as an example, and a magnetic barrier structure is added to the rotor of the motor to solve the uneven saturation problem of the rotor side magnetic bridge. This structure improves the air-gap flux density waveform of the motor by influencing the internal magnetic flux path of the motor rotor, thus improving the sine of the no-load back EMF waveform of the motor and reducing the torque ripple of the motor. At the same time, Taguchi method is used to optimize the structural parameters of the added magnetic barrier. In order to facilitate the analysis of its uneven saturation phenomenon and improve the optimization effect, a simple equivalent magnetic network (EMN) model considering the uneven saturation of rotor magnetic bridge is established in this paper, and the initial values of optimization factors are selected based on this model. Finally, the no-load back EMF waveform distortion rate, torque ripple and output torque of the optimized motor are compared and analyzed, and the influence of magnetic barrier structure parameters on the electromagnetic performance of the motor is also analyzed. The results show that the optimized motor can not change the output torque of the motor as much as possible on the basis of reducing the waveform distortion rate of no-load back EMF and torque ripple.

Index Terms—Built-in permanent magnet synchronous motor, Magnetic barrier, Taguchi method, Equivalent magnetic network model, Finite element analysis.

I. INTRODUCTION

INTERIOR permanent magnet synchronous motor (IPMSM) has the characteristics of high torque density, wide constant power operating area and low permanent magnet eddy current loss[1]-[3]. It has been widely used in the field of hybrid electric vehicles and pure electric vehicles[4]-[6]. Different from surface permanent magnet synchronous motor (SPMSM), IPM motor has asymmetric rotor, which can generate additional reluctance torque, so it has higher output torque and power

density. In addition, the permanent magnet of IPM motor is located inside the rotor, and its permanent magnet material has stronger anti-demagnetization ability than that of SPM motor. However, this rotor structure also leads to that the no-load air gap flux density waveform of IPM motor is closer to the flat top wave, and the harmonic content is much higher than that of SPM motor. There are a lot of space harmonics in the air gap of these IPM motors, which lead to higher torque ripple and additional losses when the motors are running in rated state[7]. Therefore, by reasonably improving the geometry of the stator or rotor of the motor, the harmonic components in the magnetic flux density waveform of the no-load air gap can be effectively weakened, thus reducing the torque ripple of the motor and improving the running efficiency of the motor[8]-[10].

Taguchi method is a multi-objective optimization method first proposed by Dr. Taguchi of Japan, which is widely used in various product design processes. Reference [11] uses a new systematic robust design optimization method to improve the performance of vehicle switched reluctance motor under various operating conditions. In [12], the rotor shape of rotary transformer is optimized by combining Taguchi method and finite element method. Reference [13] selected the optimal design parameter combination of synchronous generator through calculation by Taguchi method, and finally gave the optimal combination of main parameters including stator inner and outer diameter, air gap length, slot height, slot width, stator and rotor winding wire gauge and rotor offset. In reference [14], for a bearingless permanent magnet synchronous motor, in order to obtain small torque ripple, based on finite element analysis, the magnetic pole parameters were optimized by using Taguchi method orthogonal experiment. Reference [15] proposed that a Fuzzy-based sequential Taguchi robust optimization method, it has the advantages of Taguchi method, fuzzy theory and sequential optimization strategy. It is used to complete the effective robust optimization of five phase permanent magnet hub motor for electric vehicles. Reference [16] aimed at the difficulties of Taguchi method in the face of multi-objective motor optimization problems, introduced the fuzzy inference system to transform the multi-objective problem into a single objective optimization problem, and the sequential Taguchi method is used for multi-level optimization to improve the optimization accuracy.

For the interior permanent magnet synchronous motor,

Manuscript received June 28, 2022; revised August 24, 2022 and September 09, 2022; accepted September 26, 2022. Date of publication June 25, 2023; Date of current version May 11, 2023.

This work was supported by the National Natural Science Funds of China No. 51907129 and Technology program of Liaoning province No. 2021-MS-236. (*Corresponding Author: Wenming Tong*)

Shengnan Wu, Xianwen Pang, Wenming Tong and Yingcong Yao are with the School of Electrical Engineering, Shenyang University of Technology, Shenyang, 110870 China. (e-mail: imwushengnan@163.com; 944878858@qq.com; twm822@126.com).

Digital Object Identifier 10.30941/CESTEMS.2023.00018

Taguchi method is also widely used to optimize its rotor structure. Reference [17] taking a "I" IPM motor as the research object, three different magnetic barrier structures are added to the rotor of the motor, and the influence laws of adding three different magnetic barrier structures on the amplitude and torque ripple of the motor's no-load back EMF are analyzed respectively. Reference [18] also takes "I" IPM motor as an example, and studies the variation of air-gap flux density waveform distortion rate, output torque and iron loss of the motor when different magnetic barrier structures and permanent magnet chamfers are added to the rotor. In [19], the magnetic barrier structure of a U-shaped IPM motor was optimized by Taguchi method. The influence of magnetic barrier structure parameters on the output torque of the motor and the iron loss of stator and rotor under three conditions of weak magnetic speed, rated operation and overload operation of the motor was studied, and the influence weight of each magnetic barrier structure parameter was analyzed. It is concluded that the optimized magnetic barrier structure can reduce the torque ripple when the motor is loaded while reducing the iron loss. In [20], studies the magnetic barrier structure of "V- I" IPM motor, analyzes the basic structure and the improved structure schemes with magnetic barriers in various rotors by finite element software, and compares the no-load back EMF waveform distortion rate, output torque and torque pulsation of the motors under different structures. Taking these three electromagnetic performances of the motor as performance indexes, a "V- I" IPM motor with excellent performance and magnetic barrier structure is designed.

All the above documents show that reasonably adding magnetic barrier structure to the rotor of IPM motor can reduce the distortion rate of no-load air gap flux density waveform, the distortion rate of no-load back EMF waveform and torque pulsation of the motor, thus improving the stability and safety of the motor. In this paper, taking a 20kW IPM motor for vehicle as an example, a magnetic barrier structure is added to the rotor of the motor. This structure can improve the air-gap magnetic density waveform of the motor by influencing the internal magnetic flux path of the motor rotor, thus improving the sine of the no-load back EMF waveform of the motor and reducing the torque ripple of the motor. In order to analyze the unsaturated phenomenon and improve the optimization effect, a simple EMN model was built, and the structural parameters of the added magnetic barrier were optimized by Taguchi method, so that the rated output torque of the IPM motor remained unchanged after the magnetic barrier structure was added, and the influence of the structural parameters of the magnetic barrier on the electromagnetic performance of the motor was studied.

II. MATH STRUCTURE AND BASIC PARAMETERS OF BUILT-IN PERMANENT MAGNET SYNCHRONOUS MOTOR.

Fig. 1 shows the topology of the built-in permanent magnet synchronous motor, with a V-shaped rotor and a magnetic bridge structure at both ends of the permanent magnet poles. Table I shows the basic parameters of the motor.

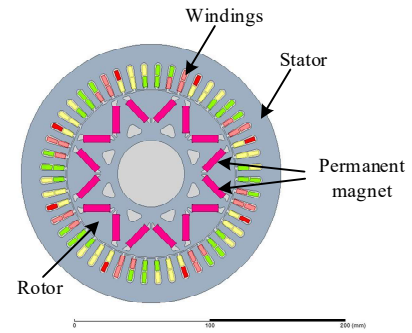


Fig. 1. Topology of the V-shape IPM Motor.

TABLE I
IPM MACHINE DETAILS

Parameter	Value
Number of poles	8
Rated current/A	89
Rated power/kW	20
Thickness of permanent magnet/mm	5
Width of permanent magnet/mm	20
Outside diameter of stator/mm	97
Rotor outer diameter /mm	62.8
Length of magnetic bridge between poles/mm	4.5
Width of magnetic bridge between poles/mm	2
Air gap length/mm	0.7
Axial length of motor/mm	75
Width of stator slot/mm	1.8
Width of stator teeth/mm	6.5

III. UNITS ROTOR STRUCTURE AND SIMPLE EMN MODEL

Fig. 2 shows the finite element simulation diagram of interior permanent magnet synchronous motor under load. From the figure, it can be seen that the magnetic bridge between poles of the motor rotor is seriously unsaturated. In order to analyze and avoid this phenomenon, the area in the figure containing the magnetic flux leakage between opposite poles is collectively called the magnetic bridge between poles. According to the geometric structure and magnetic density distribution of the magnetic bridge between poles, the magnetic bridge between poles is divided into four sub-areas, as shown in Fig. 2. It is not difficult to see that the uneven saturation mainly exists in regions 2 and 3. In order to analyze the non-uniform saturation of the magnetic bridge, a simple EMN model is built for the magnetic bridge region between the magnetic poles according to the magnetic flux path and geometry.

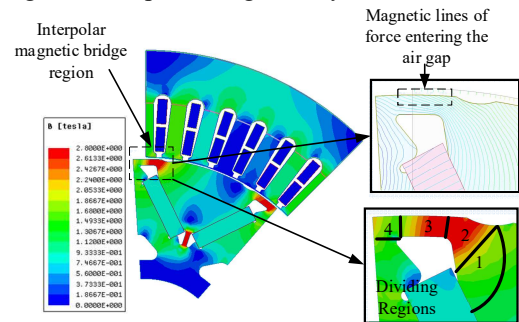


Fig. 2. Flux density distribution and division of bridge.

The established equivalent magnetic circuit model between rotor poles is shown in Fig. 3.

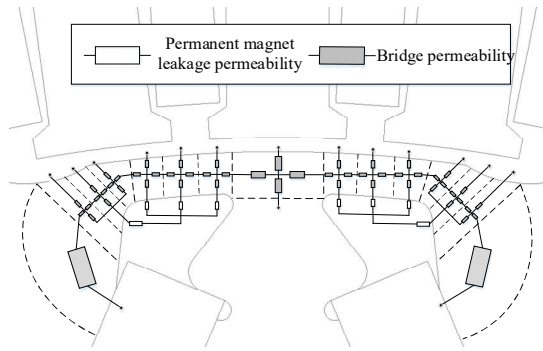


Fig. 3. EMN model of the magnetic bridge between poles.

In order to improve the saturation phenomenon of magnetic bridge between poles and reduce the no-load back EMF waveform distortion rate and torque ripple of the motor, an approximate triangular magnetic barrier structure is added to the position close to the rotor surface, as shown in Fig. 4, which shows the rotor structure of IPM motor before and after adding magnetic barrier.

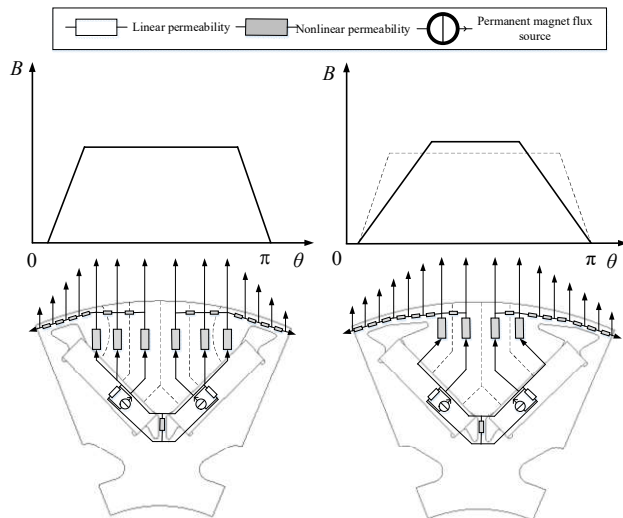


Fig. 4. The rotor magnetic flux trend before and after adding magnetic barrier and the general distribution of no-load air gap magnetic density waveform.

After adding a magnetic barrier to the IPM rotor, the magnetic flux path inside the rotor will change due to the influence of the added magnetic barrier structure, which is shown in Fig. 4 in the form of a local EMN model. According to the EMN model, the magnetic flux generated by the permanent magnet will converge to the center of the magnetic pole first, then spread to both ends of the magnetic pole after approaching the rotor surface, and then enter the air gap.

Before adding the magnetic barrier structure, the magnetic flux of the permanent magnet directly enters the air gap, and the magnetic density waveform of the no-load air gap is close to the flat top wave. After adding the magnetic barrier structure, the magnetic density waveform of the no-load air gap is closer to the sine wave. In order to verify the feasibility of this improvement scheme, finite element simulation of IPM motor before and after adding magnetic barrier is carried out, and the simulation results are shown in Fig. 5.

It can be concluded from the simulation results in Fig. 5 that the magnetic barrier structure can obviously improve the no-load air gap flux density waveform of the IPM motor.

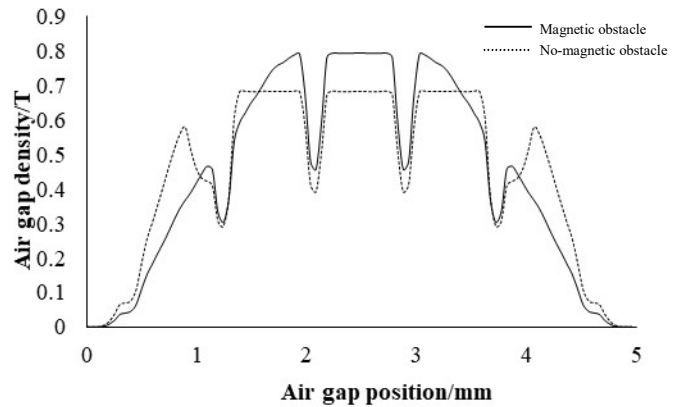


Fig. 5. No-load air gap magnetic density waveform before and after adding magnetic barrier.

However, the average output torque of the motor also decreased from the original 44.78N·m to 43.19 N m. This is because the magnetic barrier structure changes the original structure of the motor rotor, which in turn affects the d-axis inductance and q-axis inductance of the motor, and the output torque of the motor also decreases. In order to reduce the waveform distortion rate of no-load back EMF, decrease the torque ripple of IPM motor and keep its rated output torque unchanged as much as possible, in this paper, Taguchi method is used to optimize the structural parameters of the magnetic barrier. The optimization objectives include the no-load air gap flux density waveform distortion rate, no-load back EMF waveform distortion rate, torque ripple and output torque of the motor.

IV. OPTIMIZATION OF ROTOR MAGNETIC BARRIER STRUCTURE BASED ON TAGUCHI METHOD

A. Selection of Optimization Factors and Establishment of Orthogonal Table

Before the scheme design, the optimization factor of this optimization needs to be determined first, and the optimization factor in this paper is the structural parameters of magnetic barrier. The selected structural parameters must be able to determine the specific position and structure of the magnetic barrier, as shown in Fig. 6, which is the optimization factor selected for this optimization.

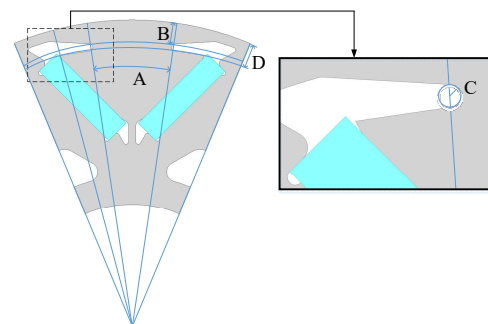


Fig. 6. Four optimization factors determining the magnetic barrier position structure

After determining the optimization factors, it is necessary to select the initial value and the range of each optimization factor. Taguchi method is a local optimization method, which can only find the optimal solution in a certain range near the initial value,

but its global optimization ability is poor. However, the local magnetic circuit model of rotor pole has the characteristics of convenient parameter modification and fast calculation speed, so the equivalent magnetic circuit model is used to screen the initial values of a large number of optimization factors. Fig. 7 shows a simple magnetic circuit model under a pair of poles after considering the magnetic barrier structure.

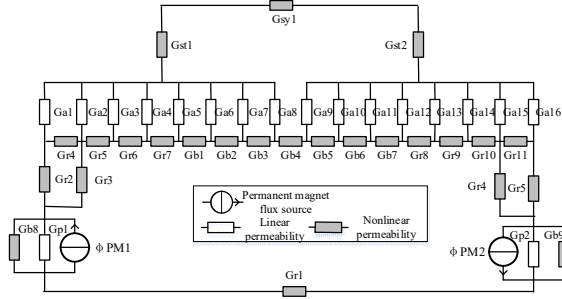


Fig. 7. EMN model for selecting initial value of optimization factor

G_{st1} and G_{st2} in the figure show the magnetic permeance of stator teeth; G_{sy1} is the magnetic permeance of the stator yoke; G_{a1} to G_{a16} are air gap permeance; G_{r1} to G_{r11} are the rotor yoke permeance; G_{b1} to G_{b9} are the permeance of rotor magnetic bridge; G_{p1} and G_{p2} are permanent magnet permeance; Φ_{PM1} and Φ_{PM2} are permanent magnet flux sources. The model ignores the cogging effect of IPM motor rotor and the influence of the new magnetic leakage path after adding magnetic barrier structure. After many experiments and calculations, the initial value and horizontal value range of the optimization factor are established by using this model. When the initial value is taken, the calculation result of EMN model for no-load air gap magnetic density is shown in Fig. 8, which shows that the result is close to sine wave waveform.

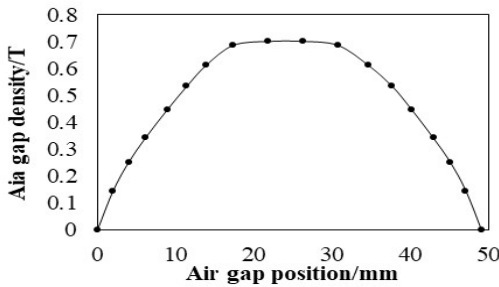


Fig. 8. Calculation results of magnetic network model when optimization factor is selected as initial value.

After the initial value of the optimization factor and the value range of the level are determined, the optimization factor level configuration table shown in Table II is established. The locations of the four optimization factors are shown in Fig. 9. If conventional methods are used to obtain the best combination of these levels, it is theoretically necessary to arrange all these combinations, respectively simulate and compare them. When the number of optimization factors and the level of optimization factors are large, the test workload will be greatly increased. There are four optimization factors in this paper, and each optimization factor has four levels. Theoretically, 256 experiments are needed to select the optimal scheme of this optimization.

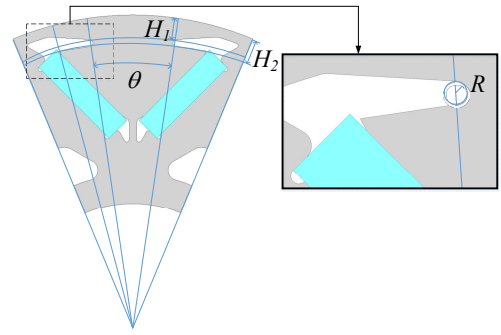


Fig. 9. Four optimization factor positions

With the same number of factors and levels, if Taguchi method is used for optimization, only 16 experiments are needed. According to Taguchi's principle, the orthogonal table of four optimization factors and four levels is established as shown in Table III. After that, only the 16 groups of schemes need to be modeled and simulated, and the final optimization scheme can be obtained by analyzing the mean value and variance of the simulation results of these schemes.

TABLE II
OPTIMIZATION FACTOR LEVEL CONFIGURATION TABLE

Optimization factor	Level 1	Level 2	Level 3	Level 4
A: $\theta(^{\circ})$	22	20.5	19	17.5
B: $H_1(\text{mm})$	2.6	2.9	3.2	3.5
C: $R(\text{mm})$	0.5	0.6	0.7	0.8
D: $H_2(\text{mm})$	3.9	4.2	4.5	4.8

TABLE III
 $L_{16}(4^4)$ ORTHOGONAL TABLE

Test number	A	B	C	D
1	1	1	1	1
2	1	2	2	2
3	1	3	3	3
4	4	4	4	4
5	2	1	2	3
6	2	2	1	4
7	2	3	4	1
8	2	4	3	2
9	3	1	3	4
10	3	2	4	3
11	3	3	1	2
12	3	4	2	1
13	4	1	4	2
14	4	2	3	1
15	4	3	2	4
16	4	4	1	3

B. Finite Element Calculation Results

The finite element simulation software is used to simulate and calculate each test combination in the orthogonal table shown in Table 3. A total of 16 groups of IPM motor models of test schemes are established. As shown in Table IV, the magnetic barrier structure of the finite element simulation model of each group of tests in orthogonal table is shown. After that, the transient simulation of the motor in each group of tests

is carried out under rated conditions, and the excitation source is powered by sine wave. As shown in Table V, the no-load air gap flux density waveform distortion rate, no-load back EMF waveform distortion rate, output torque and torque pulsation of the motor in each group of tests are obtained for the finite element method.

TABLE IV
FINITE ELEMENT MODEL OF MAGNETIC BARRIER STRUCTURE IN ORTHOGONAL TABLE

















Experimental scheme	Magnetic barrier structure	Experimental scheme	Magnetic barrier structure
1		9	
2		10	
3		11	
4		12	
5		13	
6		14	
7		15	
8		16	

TABLE V
THE RESULTS OF EXPERIMENTS IN ORTHOGONAL TABLE

Experimental scheme	Air-gap flux density distortion rate(%)	EMF distortion rate(%)	Output torque(N·m)	Torque pulsation(%)
1	20.45	2.97	44.54	6.50
2	19.53	2.48	44.43	6.53
3	18.77	2.09	44.34	6.67
4	18.29	1.80	44.26	6.34
5	21.99	2.37	44.13	6.69
6	20.45	2.06	44.18	6.25
7	18.77	1.50	43.96	6.82
8	18.21	1.37	44.01	6.68
9	23.60	1.41	43.57	7.31
10	21.34	1.09	43.51	6.91
11	19.31	1.10	43.82	6.75
12	18.14	0.91	43.76	6.80
13	24.08	42.98	7.39	7.39
14	21.20	43.19	6.95	6.95
15	20.52	43.21	6.35	6.35
16	18.77	43.38	6.18	6.18

C. Average Value Analysis

After determining the simulation results of each group of tests, it is necessary to solve the average of the four

optimization objectives. The calculation formula of the average of each optimization objective is as follows:

$$M(S) = \frac{1}{n} \sum_{i=1}^n S(i) \quad (1)$$

Where n is the total number of tests, i is the test number, S is the optimization target, and $S(i)$ is the value of the optimization target calculated from the i th test.

The optimization objectives of this optimization are no-load air gap flux density waveform distortion rate, no-load back EMF waveform distortion rate, average output torque and torque ripple, respectively. The total average results of the four optimization objectives obtained by solving the average values of the four optimization objectives by Formula (1) are shown in Table VI.

TABLE VI
TOTAL AVERAGE VALUE OF OBJECTIVES TO BE OPTIMIZED

S	Air-gap flux density distortion rate(%)	EMF distortion rate(%)	Output torque(N·m)	Torque pulsation(%)
M(S)	20.21	1.49	43.80	6.70

TABLE VII
AVERAGE VALUE OF EACH RESULT AT EACH LEVEL OF EACH FACTOR

Factor	Level	Air-gap flux density distortion rate(%)	EMF distortion rate(%)	Output torque(N·m)	Torque pulsation(%)
A	1	19.26	2.34	44.40	6.51
	2	19.86	1.83	44.07	6.61
	3	20.60	1.13	43.66	6.94
	4	21.14	0.65	43.19	6.72
B	1	22.53	1.86	43.81	6.97
	2	20.63	1.57	43.83	6.66
	3	19.34	1.34	43.83	6.65
	4	18.35	1.18	43.85	6.50
C	1	19.75	1.70	43.98	6.42
	2	20.05	1.60	43.88	6.59
	3	20.45	1.38	43.78	6.90
	4	20.62	1.27	43.68	6.87
D	1	19.64	1.51	43.86	6.77
	2	20.28	1.41	43.81	6.84
	3	20.22	1.55	43.84	6.61
	4	20.72	1.48	43.80	6.56

Then, the average value of a certain performance index of each optimization factor at some level is calculated. Taking the average value $m_{T_{avg}}(A)$ of the output torque of optimization factor A at level 1 as an example, the calculation formula is as follows:

$$m_{T_{avg}}(A) = \frac{1}{4} (T_{avg1} + T_{avg2} + T_{avg3} + T_{avg4}) \quad (2)$$

Among them, T_{avg1} 、 T_{avg2} 、 T_{avg3} and T_{avg4} are four output torque values are obtained by finite element simulation at level 1 in optimization factors A.

Similarly, the average values of the other three factors at each level can be calculated in the same way, and the calculation results are shown in Table VII. The influence of different levels of each optimization factor on each performance index can be drawn from the average value of each performance in Table VII at each level of each factor, as shown in Fig. 10.

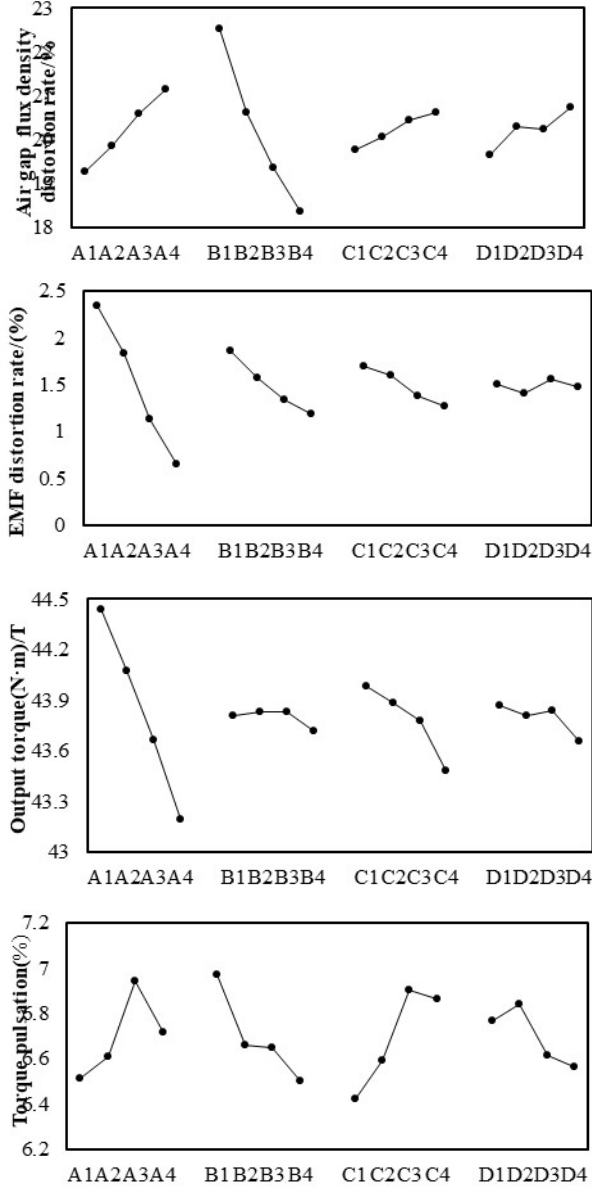


Fig. 10. Influence of different levels of each optimization factor on each performance index.

D. Variance Analysis

Variance indicates the degree to which a certain data in a set of data deviates from the total average of the set of data. In Taguchi method, by analyzing the variance of the average of a certain performance index at various levels of various factors to the total average of the performance index, we can judge the influence proportion of each optimization factor on the performance index, which is the basis for selecting the final scheme. The variance calculation formula is:

$$S_A = \frac{1}{Q} \sum_{i=1}^Q (m_{A(i)} - m_A)^2 \quad (3)$$

Where Q is the horizontal number; $m_{A(i)}$ is the average value of the performance of optimization factor A at level i ; m_A is the total average value of this performance under optimization factor A. The variance and specific gravity of each optimization factor under each performance calculated by this formula are shown in Table VIII.

TABLE VIII
VARIANCE AND SPECIFIC GRAVITY OF EACH OPTIMIZATION FACTOR UNDER EACH PERFORMANCE

Optimization factor	Air gap flux density distortion rate(%)							
	EMF distortion rate(%)		Output torque(N·m)		Torque pulsation(%)			
	variance (10 ⁻⁵)	rate	variance (10 ⁻⁵)	rate	variance (10 ⁻²)	rate	variance (10 ⁻⁵)	rate
A	5.12	15.93	4.15	81.05	20.45	92.7	0.26	23.85
B	24.40	75.89	0.64	12.5	0.11	0.50	0.30	27.52
C	1.17	3.64	0.30	5.86	1.36	6.17	0.40	36.70
D	1.46	4.54	0.03	0.59	0.14	0.64	0.13	11.93

As can be seen from Table VIII, the variation of factor A has the greatest influence on the waveform distortion rate and output torque of no-load back EMF, the variation of factor B has the greatest influence on the waveform distortion rate of no-load air gap flux density, the variation of factor C has the greatest influence on torque pulsation, and the variation of factor D has the greatest influence on torque pulsation. Therefore, the selection of factor A is based on the minimum distortion rate of no-load back EMF waveform and the minimum change of output torque. The selection of factor B is based on the minimum distortion rate of magnetic flux density waveform in no-load air gap, and the selection of factor C and factor D is based on the minimum torque ripple. It is concluded that the final optimization scheme of each factor level combination is A2B4C1D4. The values of each optimization factor are shown in Table IX.

TABLE IX
VALUE OF EACH FACTOR IN THE FINAL OPTIMIZATION SCHEME

Optimization factor	A: $\theta(^{\circ})$	B: $H_1(\text{mm})$	C: $R(\text{mm})$	D: $H_2(\text{mm})$
Value	20.5	3.5	0.5	4.8

V. OPTIMIZATION RESULT ANALYSIS

A. Performance Comparison

In order to compare the performance of the motor before and after optimization, the initial structure and the final optimized structure are simulated by finite element method, Fig. 11 is the finite element model before and after optimization. Fig. 12 shows the comparison of no-load air gap flux density waveform, no-load back EMF waveform and output torque waveform of the motor before and after optimization.

As shown in Table X, the comparison of the optimization objectives of the initial design and the final optimization scheme shows that the waveform distortion rate of the no-load

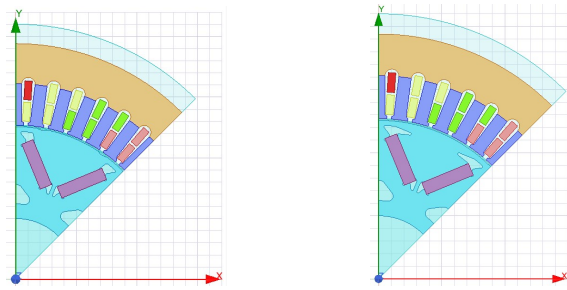


Fig. 11. Finite element model of motor before and after optimization. (a) Finite element model of initial structure motor. (b) Optimize finite element model of structural motor.

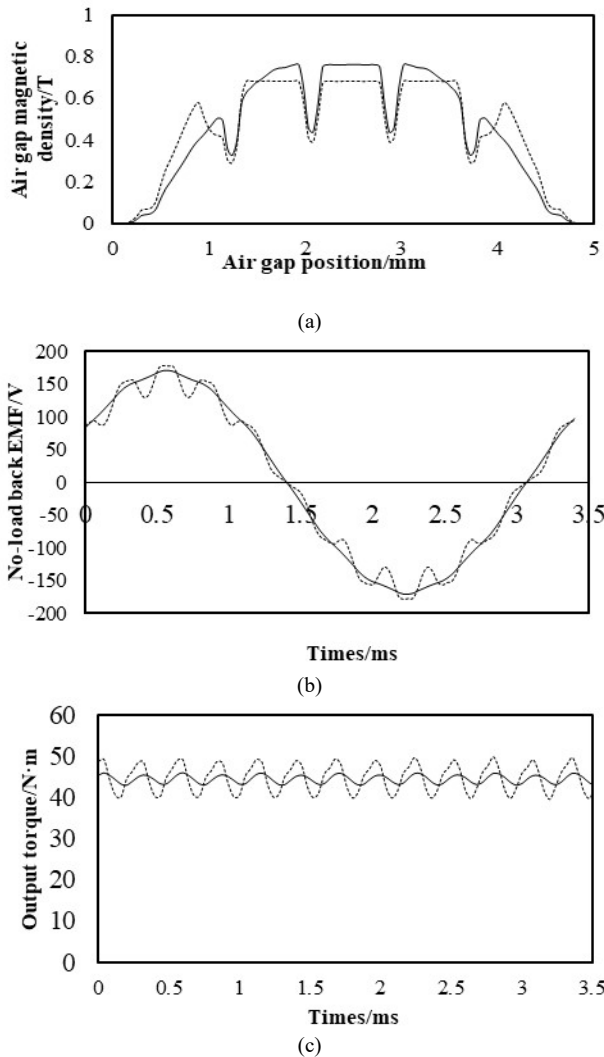


Fig. 12. Finite element simulation results of the final scheme. (a) No-load air gap flux density. (b) No-load back EMF. (c) Rated output torque.

TABLE X
COMPARISON OF OPTIMIZATION OBJECTIVES BETWEEN INITIAL DESIGN AND TAGUCHI OPTIMIZATION SCHEME

Optimization goal	Air gap flux density distortion rate(%)	EMF distortion rate(%)	Output torque(N·m)	Torque pulsation(%)
Basic structure	22.08	22.97	44.78	22.97
Optimized structure	18.4	6.84	44.45	6.84

back EMF of the optimized IPM motor is reduced from 11.42% to 1.52%, the torque ripple is reduced from 22.97% to 6.84%, and the output torque under the rated working condition is only reduced from 44.78N·m to 44.45N·m, which is only 0.74% lower than the original one.

B. Influence Law of Magnetic Barrier Structure Parameters

In this optimization process, it is found that the parameter θ of magnetic barrier structure as shown in Fig. 13 has a large proportion on both the distortion rate of no-load back EMF waveform and the output torque. This paper also studies the influence of magnetic barrier structure parameter θ on the two performance indexes of no-load back EMF waveform distortion rate and output torque of IPM motor. The results are shown in Fig. 14 and Fig. 15, where the abscissa is the ratio of θ and α in Fig. 13.

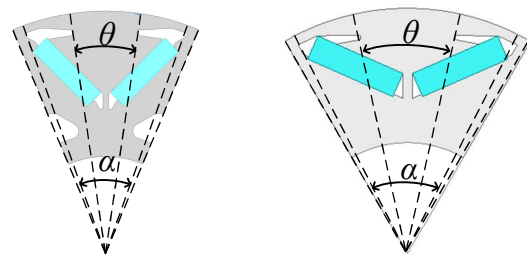


Fig. 13. Structure parameter θ of magnetic barrier.

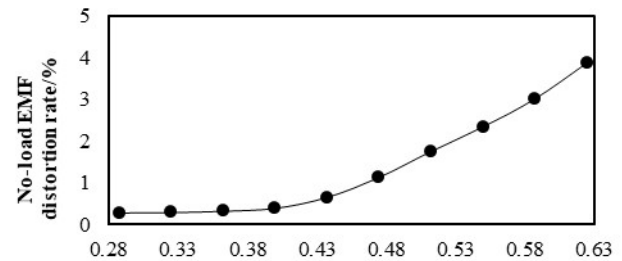


Fig. 14. Influence of the ratio of θ to α on waveform distortion rate of no-load back EMF.

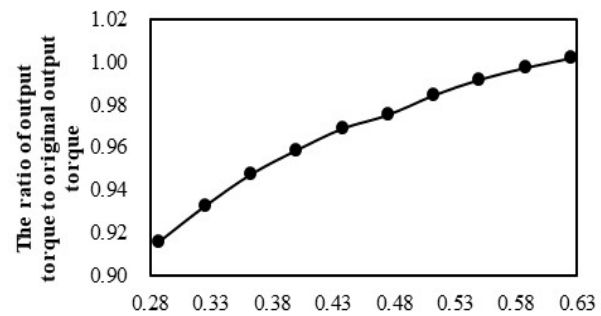


Fig. 15. Influence of the ratio of θ to α on torque

It can be seen from the figure that for the no-load back EMF of the motor, the smaller the ratio of θ to α , the smaller the waveform distortion rate of the no-load back EMF, and the smaller the waveform distortion rate of the no-load back EMF. With the decrease of the ratio, the variation of the waveform distortion rate of the no-load back EMF gradually eases. As for the output torque of the motor, the smaller the ratio of θ to α is, the smaller the output torque of the motor is, and with the decrease of the ratio, the decreasing amplitude of the output

torque of the motor keeps increasing. Therefore, the value of the magnetic barrier structure parameter θ is not as small as possible, and it needs to be reasonably selected according to the practical application of the optimized V-type IPM motor.

VI. CONCLUSION

In this paper, taking a 20kW vehicle interior permanent magnet synchronous motor as an example, the no-load back EMF waveform distortion rate and torque ripple of the motor are reduced by adding magnetic barriers to the rotor of IPM motor. The Taguchi method is used to optimize the structural parameters of the added magnetic barrier, which can reduce the waveform distortion rate and torque ripple of the no-load back EMF, while keeping the output torque of the motor under rated conditions as little as possible. In the process of optimization, in order to achieve better optimization results, a simple EMN model is used to select the initial value of optimization factors.

In addition, in the optimization process, it is found that the structure parameter θ of magnetic barrier added in this paper has a large proportion on the two performance indexes of no-load back EMF waveform distortion rate and output torque. Therefore, this paper also studies the influence law of the structure parameter θ of magnetic barrier on the two performance indexes of IPM motor, which is of positive significance to the optimal design of rotor magnetic barrier of this kind of motor.

REFERENCES

- [1] O. Ocak, M. Onsal and M. Aydan, "Development of a 7.5kW High Speed Interior Permanent Magnet Synchronous Spindle Motor for CNC Milling Machine," in *Proc. of IEEE 2018 XIII International Conference on Electrical Machines (ICEM)*, Alexandroupoli, Greece, pp. 704-709, 2018.
- [2] M. Aydin, and M. Gulec, "A New Coreless Axial Flux Interior Permanent Magnet Synchronous Motor with Sinusoidal Rotor Segments," *IEEE Transactions on Magnetics*, vol. 52, no. 7, Jul. 2016, Art. ID 8105204.
- [3] X. D. Liu, H. Chen and J. Zhao, et al. "Research on the Performances and Parameters of Interior PMSM Used for Electric Vehicles," *IEEE Transactions on Industrial Electronics*, vol. 63, no.6, pp. 3533-3545. Jun. 2016.
- [4] D. H. Wang, C. Peng, and B. D. Wang, et al. "Research on torque ripple and electromagnetic vibration suppression of a new type of permanent magnet synchronous motor with built-in rotor for electric vehicle," *Proceedings of the CSEE*, vol. 42, no. 14. pp. 5291-5299, Jul. 2022.
- [5] J. Q. Zheng, and W. X. Zhao, "Improvement Torque Performances of Interior Permanent-Magnet Machines," *CES Transactions on Electrical Machines and Systems*, vol. 3, no. 1, pp. 13-17, Mar. 2019.
- [6] T. Le, and L. J. Wu, "Driving Range Parametric Analysis of Electric Vehicles Driver by Interior Permanent Magnet Motors Considering Driving Cycles," *CES Transactions On Electrical Machines and Systems*, vol. 3, no. 4, pp. 377-381, Dec. 2019.
- [7] Y. Y. Yang, S. M. Casstano, and R. Yang, et al. "Design and Comparison of Interior Permanent Magnet Motor Topologies for Traction Applications," *IEEE Transactions on Transportation Electrification*, vol. 3, no. 1, pp. 86-97, Mar. 2017.
- [8] M. Si, X. Y. Yang, and S. W. Zhao, et al. "Optimal Design of Built-in Permanent Magnet Synchronous Motor with Spliced Rotor," *Electric Machines and Control*, vol. 21, no. 8, pp. 63-70, Aug. 2017.
- [9] K. Yamazaki, Y. Kato, and T. Ikemi, et al. "Reduction of Rotor Losses in Multilayer Interior Permanent Magnet Synchronous Motors by Introducing Novel Topology of Rotor Flux Barriers" in *Proc. of 2013 IEEE Energy Conversion Congress and Exposition*, United States, pp. 1220-1226, 2013.
- [10] Y. Dong, D. Yan, and K. Jing, et al. "Optimal Design of Low Torque Ripple Rotor of Synchronous Reluctance Motor with Gradual Magnetic Barrier," *Transactions of China Electrotechnical Society*, vol. 32, no. 19, pp. 22-30, Oct. 2017.
- [11] K. K. Diao, X. D. Sun, and G. Lei, et al. "System-level Robust Design Optimization of a Switched Reluctance Motor Drive System Considering Multiple Driving Cycles," *IEEE Transactions on Energy Conversion*, vol. 36, no. 1, pp. 348-357, Mar. 2021.
- [12] L. F. Xiao, Z. Li, and C. Bi, "An Optimization Approach to Variable Reluctance Resolver," *IEEE Transactions on Magnetics*, vol. 56, no. 2, pp. 1-5, Feb. 2020.
- [13] P. Cheng, X. J. Yang, and H. Lan, et al. "Design and Efficiency Optimization of Synchronous Generator Based on Finite Element Method and Taguchi Method," *Electric Machines and Control*, vol. 23, no. 2, pp. 95-99, Feb. 2019.
- [14] H. Q. Zhu, and Y. F. Cheng, "Rotor Optimization Design of Bearingless Permanent Magnet Synchronous Motor Based on Combined Magnetic Pole," *Electric Machines and Control*, vol. 24, no. 3, pp. 124-130, Mar. 2020.
- [15] S. Zhou, X. D. Sun, and Y. F. Cai, et al. "Robust Design Optimization of a Five-phase PM Hub Motor for Fault-tolerant Operation Based on Taguchi Method," *IEEE Transactions on Energy Conversion*, vol. 35, no. 4, pp. 2036-2044, Dec. 2020.
- [16] X. D. Sun, Z. Shi, and J. G. Zhu, "Multiobjective Design Optimization of an IPMSM for Evs Based on Fuzzy Method and Sequential Taguchi Method," *IEEE Transactions on Industrial Electronics*, vol. 68, no. 11, pp. 10592-10600, Nov. 2021.
- [17] K. Kim, D. Koo, and J. Hong, et al. "A Study On The Characteristics Due to Pole-Arc to Pole-pitch Ratio and Saliency to Improve Torque Performance of IPMSM," vol. 43, no. 6, pp. 2516-1518, Jun. 2007.
- [18] K. Yamazaki, and H. Ishigami, "Rotor-shape Optimization of Interior-permanent-magnet Motors to Reduce Harmonic Iron Losses," *IEEE Transactions on Industrial Electronics*, vol. 57, no. 1, pp. 61-69, Jan. 2010.
- [19] C. L. Xia, L. Y. Guo, and Z. Zhang, et al. "Optimal Designing of Permanent Magnet Cavity to Reduce Iron Loss of Interior Permanent Magnet Machine", *IEEE Transactions on Magnetics*, vol. 51, no. 12, pp. 1-9, Dec. 2015.
- [20] K. Yamazaki, M. Kumagai, and T. Ikemi, et al. "A Novel Rotor Design of Interior Permanent-magnet Synchronous Motors to Cope with Both Maximum Torque and Iron-loss Reduction," *IEEE Transactions on Industry Applications*, vol. 49, no. 6, pp. 2478-2486, Nov. 2013.



Shengnan Wu (M'18) was born in Yingkou, China. She received the B.S., M.S., and Ph.D. degrees in electrical engineering from the Shenyang University of Technology, Shenyang, China, in 2008, 2011, and 2017, respectively.

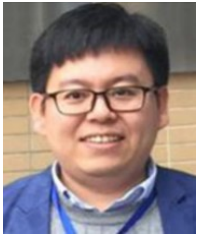
She is currently a Postdoctoral Research Assistant in electrical engineering with Shenyang University of Technology. Her research interests include electromagnetic design and multiphysical field simulation and analysis of permanent magnet machines.



Xianwen Pang was born in Inner Mongolia, China. He received his bachelor's degree in electrical engineering from Shenyang University of technology in Shenyang, China in 2020. Currently, he is studying for a master's degree in electrical engineering at Shenyang University of technology in China.

His main research interests include the

design and optimization of hybrid excitation motor and permanent magnet motor.



Wenming Tong (M'18) was born in Dandong, China. He received the B.S. and Ph.D. degrees in electrical engineering from the Shenyang University of Technology, Shenyang, China, in 2007 and 2012, respectively. He is currently an Associate Professor with the National

Engineering Research Center for Rare Earth Permanent Magnet Machines, Shenyang University of Technology.

His major research interests include the design, analysis, and control of high-speed and low-speed direct drive permanent magnet machines, axial flux permanent magnet machines, hybrid excitation machines, and high-performance machines with new types of soft magnetic materials.



Yingcong Yao was born in Zhejiang, China. He received a master's degree in electrical Master of Engineering from Shenyang University of Technology in Shenyang, China in 2021. At present, he is studying for a master's degree in electrical Master of Engineering at Shenyang University of Technology.

His main research interest is the design and optimization of permanent magnet synchronous motors.